

A multi-messenger mass determination method for LISA Neutron-Star–White-Dwarf Binaries

KAYE JIALE LI ¹, JANE SINAN LONG ^{2,*}, KINWAH WU ^{1,2} AND ALBERT K. H. KONG ²

¹ Mullard Space Science Laboratory, University College London, Holmbury St Mary, Surrey, RH5 6NT, United Kingdom

² Institute of Astronomy, National Tsing Hua University, Hsinchu 30013, Taiwan (ROC)

ABSTRACT

Determining the mass of the neutron stars (NSs) accurately improves our understanding of the NS interior and complicated binary evolution. However, the masses of the systems are degenerate with orbital inclination angle when using solely gravitational waves (GWs) or electromagnetic measurements, especially for face-on binaries. Taking advantages of both GWs and optical observations for LISA neutron-star–white-dwarf (NS-WD) binaries, we propose a mass determination method utilising multi-messenger observational information. By combining the binary mass function obtained from optical observations and a GW mass function, that we introduce, derived from GW observations, we demonstrate how we can set improved constraints on the NS mass and break the degeneracy in the mass and viewing inclination determination. We further comment on the universal relation of the error bar of the GW mass function versus GW signal-to-noise ratio (SNR), and propose a simple method for the estimate of capability of GW observations on mass determination with LISA. We show that for ultra-compact NS-WD binaries within our Galaxy, the mass of the NS can be constrained to within an accuracy of $\pm 0.2 M_{\odot}$ with the proposed method.

1. INTRODUCTION

Neutron stars (NSs) are composed of the densest matter known to date, and their mass density is inaccessible in laboratory experiments. The masses of NS are around $1 - 2 M_{\odot}$, and their upper limit is set by the ability of the forces of quantum nature to counteract the NS's self-gravity. Observations have revealed several massive ($\gtrsim 2 M_{\odot}$) NSs in the neutron-star-white-dwarf (NS-WD) binaries (Demorest et al. 2010; Antoniadis et al. 2013; Cromartie et al. 2020; Fonseca et al. 2021). These observations have challenged the existence of exotic matter, which typically softens the equation of state (EOS) compared to pure nucleonic matter, thereby lowering the maximum mass a NS can support (Baldo et al. 2000; Vidana et al. 2011; Moshfegh & Ghazanfari Mojarrad 2013). A large parameter space for such exotic matter has been ruled out or at least disfavored (see e.g. Demorest et al. 2010; Pang et al. 2021). However, models incorporating a condensed quark core remain viable (Tang et al. 2021; Li et al. 2021; Akmal et al. 1998a; Alford et al. 2013), and factors such as many-body corrections to baryon-baryon interactions (Akmal et al. 1998b; Zhou et al. 2004; Li & Schulze 2008; Ghazanfari

Mojarrad & Arabsaeidi 2016), magnetic fields (Zurairq et al. 2023), differential rotation (Espino & Paschalidis 2019), and finite temperatures (Lattimer & Swesty 1991) could alter the upper mass limit. Firmly establishing the mass values for the heaviest NSs will tighten the constraints on the allowed EOS of dense matter and hence the structural models and the internal compositions of the NS family (Lattimer & Prakash 2004, 2007). It also gives us a means to study the behaviours of complex phases of dense quantum matter under extreme pressure and gravity (Avancini et al. 2008; Baym et al. 2018; Tan et al. 2022).

Compact NS-WD binaries in our Galaxy are candidate sources for the space-borne gravitational wave (GW) detector LISA. They could be formed through several channels. For instance, some may descend from low-mass/intermediate-mass X-ray binaries (LMXBs/IMXBs), consisting of a NS accreting matter from a low- or intermediate-mass giant (see e.g. Tauris & Savonije 1999) or even a degenerate WD companion (see e.g. Tutukov & Yungel'Son 1993). They may also be products of dynamical few-body interactions occurring in very dense stellar environments, e.g. cores of dense stellar clusters. The Galactic population of NS-WD binaries is highly uncertain. It is estimated to range from a few to a few hundreds within LISA detection sensitivity, based on population synthesis models or X-ray luminosity function (Nelemans et al. 2001; Benacquista et al. 2001; Cooray 2004; Chen et al. 2020; Korol et al. 2023). The NS-WD binaries, be they in the detached or semi-detached configuration, with orbital evo-

Corresponding author: Jane SiNan Long (JSL), Kaye Jiale Li (KJL), Albert, K. H. Kong (AKHK)

sinan.long.23@ucl.ac.uk (JSL), j-li.19@ucl.ac.uk (KJL), akong@gapp.nthu.edu.tw (AKHK)

* Present Address: Mullard Space Science Laboratory, UCL

lution driven by the angular momentum loss through gravitational radiation (see Paczyński 1971), can provide clean constraints to the masses of component stars through multi-messenger observations. The compact nature of the WD companion allows the NS-WD binaries to remain detached, even when their orbital period, P_{orb} , evolves to as short as about $\lesssim 10$ min (Tauris 2018; Yu et al. 2021; Chen et al. 2021, 2022). These NS-WD binaries naturally emit GWs. The frequencies of their GWs are expected to be from 0.5 mHz to 3 mHz, which fall within the detectable range of the LISA (see Amaro-Seoane et al. 2017). Multi-messenger observations of NS-WD binaries in GW and electromagnetic (EM) waves will give us the opportunities to probe the physics of high-density matter in strong gravity in addition to enhancing our understanding of the nature, the dynamics and the origins of NS-WD binaries.

The focus of this study is to derive tighter constraints on the masses of the NSs in NS-WD binaries detectable by LISA. We specifically introduce a GW mass function, which is constructed using the information from GW observations. This is complementary to the conventional binary mass function which is derived from optical photometry or spectroscopy or other EM/photonic observations. We use the GW analysis pipeline *gbmcmc* (Littenberg et al. 2020a) to generate mock LISA data for parameter estimations. Using the results from the Markov Chain Monte Carlo (MCMC) sampling and the two mass functions, which are almost diagonal, we can constrain the orbital inclinations and hence establish the masses of the NSs. We organise the paper as follows. The methodology and the procedures are presented in §2 and the results in §3. We discuss our findings in §4. We also comment on the astrophysics of the target binaries. A short summary is given in §5.

2. METHOD

2.1. SNR threshold for gravitational-wave sources

Consider a binary system consisting of a NS of m_{ns} and a low-mass WD of m_{c} orbiting around each other with a period P_{orb} . The orbital revolution of the binary leads to the emission of GW, and the GW is characterised by a frequency $f_{\text{GW}} \equiv 2/P_{\text{orb}}$. The loss of orbital energy and angular momentum caused by the GW emission bring the stars in the binary closer, which in turns shortens P_{orb} , and increases f_{GW} . The rate of change in f_{GW} is given by

$$\begin{aligned} \dot{f}_{\text{GW}} &= \frac{96}{5} \frac{G^{5/3}}{c^5} \pi^{8/3} \mathcal{M}^{5/3} f_{\text{GW}}^{11/3} \\ &\approx 1.8 \times 10^{-11} \left(\frac{\eta}{0.3} \right) \left(\frac{M}{2.6 M_{\odot}} \right)^{5/3} \left(\frac{1 \text{ hr}}{P_{\text{orb}}} \right)^{11/3} \text{ Hz yr}^{-1} \end{aligned} \quad (1)$$

(see e.g. Maggiore 2008), where $M = m_{\text{ns}} + m_{\text{c}}$ is the total mass of the binary, $\eta = (m_{\text{c}} m_{\text{ns}}) / (m_{\text{ns}} + m_{\text{c}})^2$ is the symmetric

mass ratio, and

$$\mathcal{M} \equiv \frac{(m_{\text{c}} m_{\text{ns}})^{3/5}}{(m_{\text{ns}} + m_{\text{c}})^{1/5}}, \quad (2)$$

is the chirp mass.

For the parameters of interest in this study, the drift in frequency is about $\Delta f_{\text{GW}} \approx 1 \times 10^{-11}$ Hz over a period of 4 yr (expected LISA mission lifetime). This value is much smaller than f_{GW} . The GW from the system is therefore practically quasi-monochromatic. Following Finn & Thorne (2000), we define the characteristic amplitude of the GW as $h_{\text{c}} \equiv h_{\text{o}} \sqrt{2f^2/\dot{f}}$, where $h_{\text{o}} \equiv \sqrt{\langle h_{+}^2 + h_{\times}^2 \rangle} = I(\iota) \sqrt{G\dot{E}/c^3}/(\pi df)$ is the rms amplitude of the two polarisations averaged over one GW period. The prefactor $I(\iota)$ accounting for the effect of the inclination angle, which is the rms of the angular part of h_{+} and h_{\times} , is given by

$$I(\iota) \equiv \sqrt{\frac{5}{4}} \sqrt{\cos^2 \iota + \left(\frac{1 + \cos^2 \iota}{2} \right)^2}, \quad (3)$$

which is normalised such that $\int (d\Omega/4\pi) I^2(\iota) = 1$. The signal-to-noise ratio (SNR) of this quasi-monochromatic GW is

$$\text{SNR} = \sqrt{\int_{-\infty}^{\infty} d(\ln f) \left(\frac{h_{\text{c}}(f)}{h_{\text{n}}(f)} \right)^2} \approx \frac{\sqrt{2fT} h_{\text{o}}}{h_{\text{n}}(f)} \quad (4)$$

(Flanagan & Hughes 1998; Finn & Thorne 2000; Moore et al. 2015; Robson et al. 2019), where $h_{\text{n}}(f) \equiv \sqrt{f S_{\text{n}}(f)}$ is the sky-averaged rms noise at frequency f , and T is the observational time. $S_{\text{n}}(f)$ is the one-sided, sky-averaged power spectral density (PSD) of the detector at frequency f .

We may take the sensitivity curve as

$$\begin{aligned} S_{\text{n}}(f) &= \frac{10}{3L^2} \left\{ P_{\text{OMS}} + 2 \left[1 + \cos^2 \left(\frac{f}{f_*} \right) \right] \frac{P_{\text{acc}}}{(2\pi f)^4} \right\} \\ &\quad \times \left[1 + \frac{6}{10} \left(\frac{f}{f_*} \right)^2 \right] \end{aligned} \quad (5)$$

(Robson et al. 2019). Here, $L = 2.5$ Gm and $f_* = c/(2\pi L) = 19.09$ mHz. The single test mass acceleration noise single-link optical metrology noise P_{acc} and P_{OMS} are then

$$\begin{cases} P_{\text{acc}} = 9 \times 10^{-30} \left[1 + \left(\frac{0.4 \text{ mHz}}{f} \right)^2 \right] \left[1 + \left(\frac{f}{8 \text{ mHz}} \right)^4 \right] \frac{\text{m}^2}{\text{Hz s}^4}; \\ P_{\text{OMS}} = 2.25 \times 10^{-22} \left[1 + \left(\frac{2 \text{ mHz}}{f} \right)^4 \right] \frac{\text{m}^2}{\text{Hz}}, \end{cases} \quad (6)$$

so to be consistent with the *gbmcmc* package used in this study¹.

¹ The noise parameters are adapted from LISA LDC git:<https://gitlab.in2p3.fr/LISA/LDC/-/blob/master/ldc/lisa/noise/noise.py>

Based on the formula of SNR in Eq. 4, we define an effective GW strain $h_e = \sqrt{2fT} h_o = \sqrt{2N_{\text{cyc}}} h_o$, where N_{cyc} is the number of wave cycles detected within observational time T , which is the same as that adopted in Chen et al. (2020). The effective GW strain is then

$$\begin{aligned} h_e &= I(t) \sqrt{2N_{\text{cyc}}} \frac{1}{\pi df} \sqrt{\frac{G\dot{E}}{c^3}} \\ &= I(t) \frac{8}{\sqrt{5}} \frac{G^{5/3}}{dc^4} \pi^{2/3} \mathcal{M}^{5/3} f^{2/3} \sqrt{N_{\text{cyc}}} \\ &\approx 3 \times 10^{-20} I(t) \left(\frac{30 \text{ min}}{P_{\text{orb}}} \right)^{7/6} \left(\frac{\mathcal{M}}{(2/5)^{1/5} M_{\odot}} \right)^{5/3} \\ &\quad \times \left(\frac{T}{4 \text{ yr}} \right)^{1/2} \left(\frac{10 \text{ kpc}}{d} \right), \end{aligned} \quad (7)$$

and the SNR can be visually determined by how far this effective strain is above the noise amplitude $h_n(f)$.

While it is conventional to set $\text{SNR} = 5$ as the criterion of detection, this threshold is merely representative. Depending on the (time-delay interferometry) TDI channels considered, whether sky-averaged has been performed and how is it performed, the amplitude of the Galactic confusion noise, and whether the orbital orientation is averaged out, the SNR value of the exact same system could differ by a factor of a few. For example, the package `gbmcmc` (Littenberg et al. 2020a) has a more detailed definition of SNR (see Littenberg & Cornish 2019) using a combination of A and E channel with realistic responses to different sky locations, polarization, and inclination angles. For simplicity, we have considered two X -channels and averaged over the source’s sky position and detector orientation angle. For the system we considered in this work, our SNR definition in Eq. 4 is consistent in number with $\text{SNR}(\text{gbmcmc})$, with a difference of $\leq 20\%$, mainly depending on the sky position. To account for this subtle difference in definition across literature, we relax this criterion to $\text{SNR} = 2$ and consider a wider range of systems, including those with $2 < \text{SNR} < 5$. Nevertheless, the SNR (or sometimes $\text{SNR}(\text{gbmcmc})$ as calculated by the `gbmcmc` package) of each system will be listed to indicate the possibility of it being detected.

In this study, we consider NS-WD binaries with orbital period $P_{\text{orb}} = 10 - 60$ min, which is within LISA’s sensitivity range. The parameter choice extends toward lower frequencies, as systems with longer periods have longer lifetimes compared to more compact systems, thus dominating the population. The distance range for these systems is chosen to be $d = 1 - 30$ kpc, covering our entire Galaxy. In particular, we choose hypothetical systems very close by to study parameter degeneracy and demonstrate the universality of our findings for high SNR systems. The existence of such systems within our Galaxy is discussed in Sec. 4.2. Without losing generality we assume that the binary has a circular orbit. The

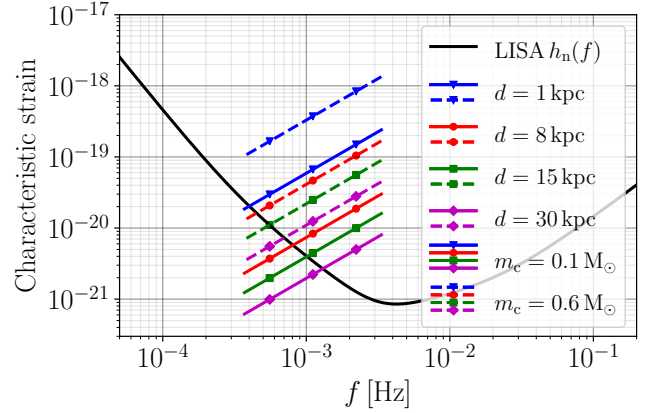


Figure 1. The range of inclination angle-averaged effective GW strain of the binary system with $m_{\text{NS}} = 2.0 M_{\odot}$ and $m_c = 0.1, 0.6 M_{\odot}$ at $d = 1, 8, 15,$ and 30 kpc. Each line represents a specific type of binary system of the same m_c and d , with orbital period P_{orb} spanning from 10 min to 90 min. The three nodes are marked at $P_{\text{orb}} = 60, 30, 15$ min from left to right respectively. The integration time of the observations is set to be 4 years. LISA sensitivity curve is defined in Eq. 5.

mass of the NS is $2 M_{\odot}$ ² and the mass of the companion star is within the range $m_c = 0.1 - 0.6 M_{\odot}$, although the majority of our results can be extended to a wider parameter range. Fig. 1 illustrates the effective GW strains of the NS-WD binaries, for a range of distances, orbital periods, and companion masses. The LISA sensitivity curve is included in the graph for comparison.

2.2. Parameter estimation method

NS-WD binaries have the potential to be identified through EM observations before LISA is launched, contributing to the family of verification binaries for LISA (Stroeer & Vecchio 2006; Korol et al. 2017; Kupfer et al. 2018; Burdge et al. 2019a,b, 2020; Kilic et al. 2021; Johnson et al. 2023; Finch et al. 2023; Kupfer et al. 2023). Alternatively, if the WD companion is too faint for detection in optical surveys, GW observations could offer localisation information for the binary, enabling targeted follow-up searches. In this study, we assume that the binary has been identified through optical observations, either before or after GW identification. Through spectroscopic analysis, supplemented with photo-

² The existence of $2 M_{\odot}$ NSs is supported by observations of NS-WD binaries (Demorest et al. 2010; Antoniadis et al. 2013; Cromartie et al. 2020; Fonseca et al. 2021) which motivates our choice of this value. In the literature, $2 M_{\odot}$ is often used as a benchmark to identify the existence and properties of exotic matter (Lattimer & Prakash 2010; Akmal et al. 1998b). However, exotic matter can still support NS exceeding $2 M_{\odot}$, with a critical threshold likely a few tenths of a solar mass higher – though this remains highly model-dependent and complex (see e.g. Char & Banik 2014; Zuraik et al. 2023). For simplicity, we adopt this convention while noting that our main result is insensitive to the specific choice.

metric analysis, the orbital periods P_{orb} and phase resolved radial velocities K of the WD are measured and are then used to construct the binary mass function,

$$f(m) = \frac{P_{\text{orb}} K^3}{2\pi G} = \frac{m_{\text{ns}}^3 \sin^3 \iota}{(m_{\text{ns}} + m_c)^2}. \quad (8)$$

Currently there has been no confirmed identifications of our target compact (10–60 min) NS-WD binaries³. Estimating the uncertainty in determining the binary mass function poses a non-trivial challenge. This uncertainty arises from factors such as the data quality, as well as the modeling the WD’s brightness variations due to tidal effects and/or pulsar irradiation. Given these complexities, we find it impractical to estimate the uncertainty directly for an unspecified system over a multi-dimension parameter space. Instead, focusing on GW observations, we assign specific values to the binary mass function uncertainty (i.e. 5 – 20%) to assess the sensitivity of mass estimates under these conditions.

For the GW part, we made use of the package `gbmcmc` (Littenberg et al. 2020b) to perform mock parameter estimation of such binary systems with different inclination angles, orbital periods, and distances. Each binary is fitted with typically eight parameters including orbital frequency f , frequency derivative \dot{f} , GW amplitude A , inclination angle ι , polarisation angle ψ , initial orbital phase ϕ of GW and sky localization, where

$$A \equiv \frac{2}{d} \frac{G^{5/3}}{c^4} (\pi f)^{2/3} \mathcal{M}^{5/3}. \quad (9)$$

We have excluded noise in the mock data so as to derive a clearer degeneracy between system parameters. In this analysis, we have assumed such a system to be readily detected via EM observations with known sky location and orbital frequency, and hence f . The prior of polarisation angle and initial orbital phase is uniform in $[0, \pi]$ and $[0, 2\pi]$, respectively. We restrict our study to prograde orbit and set the prior on the inclination angle such that $\cos \iota$ is uniform in $[0, 1]$. The prior amplitude A is log-uniform between $\ln A = -60$ and $\ln A = -45$.

³ The absolute brightness of white dwarfs is $M_V \sim 11.5$ (see e.g. Micaelien et al. 2022). This corresponds to the visual magnitude $V \approx 26$ at a distance of 8 kpc. The 8-m class ESO Very Large Telescopes (VLT) are capable of observing source of $V \approx 27$ with sensible SNR at an integration time of 1 hr (see Reddy et al. 2019). While observation for our target NS-WD binaries at distance exceeding about 4 kpc with reliable photometric determination of periodic variations is beyond the capacity of current ground-based telescopes, with the coming of the 30-m class telescopes, such as the Extremely Large Telescope (ELT) and the Thirty Meter Telescope (TMT), resolving 10 min photometric variations at $V \approx 26$ would be achievable for hours of integration time. The simple estimate above has not taken account of important local effects, such as night-sky brightness and atmospheric scintillations. All these would restrict the size of observational volume for the target binaries to reside. We may be able to circumvent these in space-base observations, where night-sky brightness, seeing, and other atmospheric effects would not be present.

In the mock parameter estimation, the system is assumed to be located at $\sin(\text{latitude}) = 0.6080$ and longitude = 2.9737 in solar system barycenter ecliptic coordinates and it consists of a NS with $2 M_{\odot}$ and a companion with $m_c = 0.1 - 0.6 M_{\odot}$, with an observational duration of the GW signal of 4 yr. The system is assumed to have negligible accretion such that $\dot{f} = \dot{f}_{\text{GW}} \ll f/4 \text{ yr}$ and the source is essentially monochromatic. In this study, we aim at demonstrating the capability of GW observations, and hence have adopted a simplified model by assuming that the companion mass and binary distance are known a priori from previous EM observations (see Appendix A for a detailed discussion). With the information of m_c and distance d known, the mass of the NS can be exactly determined from a given A by combining Eq. 2 and Eq. 9. In practice, both the companion mass and the distance would be measured with an error bar. For such a monochromatic source, the distance is completely degenerate with the chirp mass. Therefore, the uncertainty of distance can be translated into the uncertainty of GW chirp mass via error propagation.

The error propagation for companion mass is more subtle as it appears in both the binary mass function and GW amplitude. We will show how the error of companion mass affects the error of the NS’s mass in appendix A.

While it is straightforward to calculate the system’s chirp mass from GW amplitude A using Eq. 9, A is not necessarily a good parameter due to its degeneracy with the inclination angle in GW detection. The two observed polarisation modes $h_+ \propto A(1 + \cos^2 \iota)/2$ and $h_{\times} \propto A \cos \iota$, suggest that a system with larger A and larger inclination angles can be mistaken as a system with smaller A and smaller inclination angles. Significant degeneracy appears even for signals with large SNR when the system is close to face-on. For example, Fig. 2 shows the parameter estimation for an unrealistic injected signal emitted by a binary with $m_c = 0.5 M_{\odot}$, $P_{\text{orb}} = 15 \text{ min}$, $\cos \iota = 0.9$ at a distance of 3 kpc. This system has $\text{SNR} \approx 260$ after a 4-year integration time. The parameter estimation for such a luminous system is expected to be very precise, but as shown by the 1D marginalized probability density function (PDF) of A and $\cos \iota$, both PDFs differ significantly from a bell-shaped distribution and the locations of maximum posteriors mismatch the true values. This degeneracy motivates the definition of a new parameter that combines the information of both amplitude and inclination angle.

We define a GW mass function from GW measurement, similar to the binary mass function from measurements of

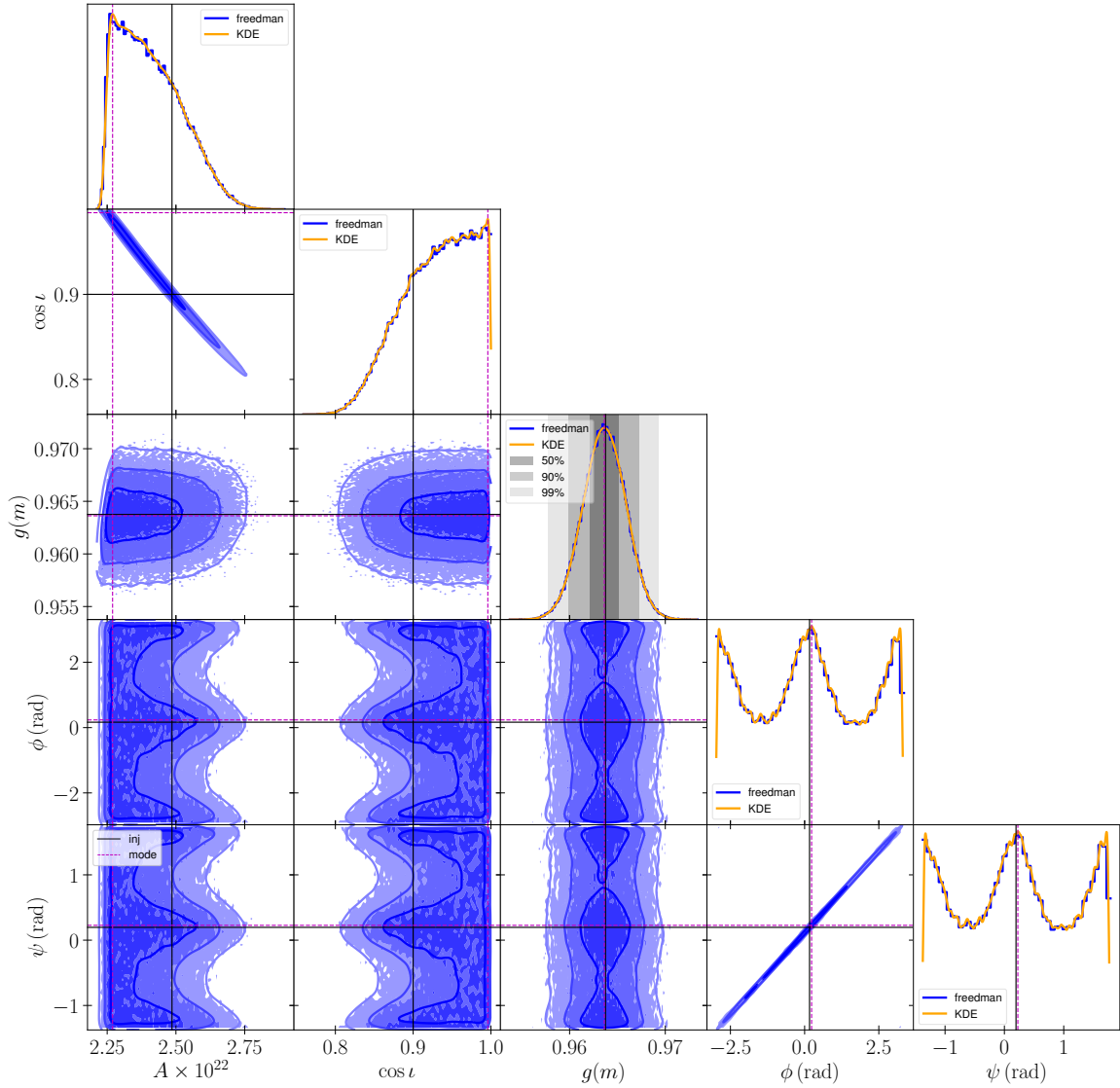


Figure 2. The parameter estimation of the GW emitted by a binary system with $m_c = 0.5 M_\odot$, $P_{\text{orb}} = 15$ min, and $\cos i = 0.9$ (nearly face-on) located at 3 kpc away. The detection time is 4-year. The SNR of this system is ≈ 260 . The contour lines represent the 50%, 90%, and 99% confidence intervals. The histogram is calculated using the *astropy* package (Astropy Collaboration et al. 2022a) and the kernel density estimation (KDE) is calculated by *getdist* package (Lewis 2019).

radial velocity variation (e.g. Eq. 8), as

$$\begin{aligned}
 g(m) &= \left[\frac{Ad}{2(\pi f)^{2/3}} \frac{c^4}{G^{5/3}} \sqrt{\cos^2 i + \left(\frac{1 + \cos^2 i}{2} \right)^2} \right]^{3/5} \\
 &= \frac{(m_{\text{ns}} m_c)^{3/5}}{(m_{\text{ns}} + m_c)^{1/5}} \left[\cos^2 i + \left(\frac{1 + \cos^2 i}{2} \right)^2 \right]^{3/10}. \quad (10)
 \end{aligned}$$

Similar to that of the binary mass function, the first equal sign shows how the GW mass function is derived from direct observation parameters, while the second equal sign indicates its relation with the intrinsic binary parameters. Here, A and $\cos i$ are obtained from GW parameter estimation, while f and d are known a priori from EM observations. This GW mass function is proportional to $\langle h_+^2 + h_\times^2 \rangle^{3/10}$, taking into account the fact that LISA measures a combination of h_+ and h_\times as it rotates in space. As shown in the bottom-right

panel of Fig. 2, the PDF of the GW mass function has a nice symmetrical bell-shape, as opposed to the PDFs of A and $\cos i$ which are not as meaningful when viewed individually.

The GW mass function admits advantages in the parameter estimation that involves multi-messenger observations regardless of the orbital configuration of the NS-WD binary. The accuracy of parameter estimation of $g(m)$ follows a simple relation with the SNR of the binary system, particularly at high SNRs. Fig. 3 compares the accuracy on the parameter estimation for A and $g(m)$ achievable for the NS-WD binaries. Compared with that of A , the relative size of the confidence interval (i.e. the error bar) of $g(m)$ roughly follows a power law relation with the SNRs of the system. We define $g(m)_{\text{max,min}} = g(m)_0(1 \pm \delta_{\text{gm}})$, such that $g(m)_0$ represents the true value of the GW mass function. The averaged relative error of δ_{gm} is reasonably well fitted by the following

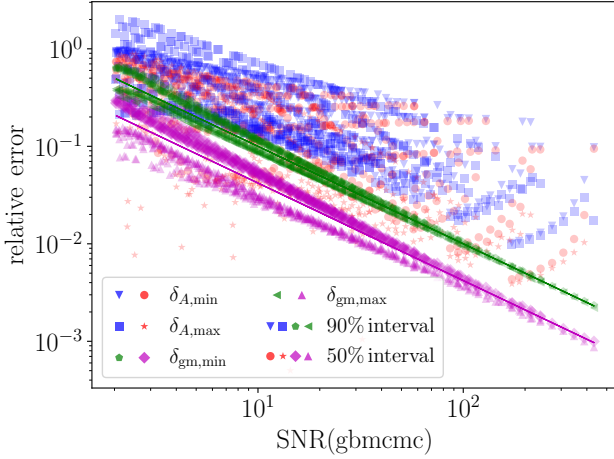


Figure 3. The relative error of the parameter A and $g(m)$ versus the SNR of the system, at a confidence interval of 50% and 90% respectively. The upper and lower error bar of $g(m)$ is defined as $\delta_{gm,max} \equiv (\max g(m) - g(m)_0)/g(m)_0$, $\delta_{gm,min} \equiv (g(m)_0 - \min g(m))/g(m)_0$, and similarly for A . Some $\delta_{A,max}$ values are missing as the strong degeneracy between A and $\cos \iota$ has led to $\max A < A_0$, as demonstrated in Fig. 2. The relative errors of $g(m)$ roughly follow power law relation with respect to SNR whereas the error bars of A have large scatters. The solid lines represent the power-law relation reported in Eq. 11, which are derived by fitting the average of the maximum and minimum relative errors. The data shown are calculated with $m_c = 0.6 M_\odot$ and $P_{orb} = 20 - 60$ min, although the results for other masses and orbital periods are very similar.

relations:

$$\begin{cases} \delta_{gm,50\%} \approx 0.042 \left(\frac{10}{\text{SNR}} \right); \\ \delta_{gm,90\%} \approx 0.10 \left(\frac{10}{\text{SNR}} \right), \end{cases} \quad (11)$$

which are appropriate for NS-WD binaries with $\text{SNR} \in [3, 400]$. This relation has been validated across a range of companion masses, distances, inclination angles ($\cos \iota = 0.1 - 0.9$), orbital periods ($P_{orb} = 10 - 60$ min) and amplitudes ($A \in [3 \times 10^{-23}, 7 \times 10^{-22}]$), provided the SNR falls within this range. However, caution is advised when applying this relation, as elaborated at the end of this section. As shown in Fig. 3, the relative error of $g(m)$ is almost always smaller than that of A at the same confidence interval. For a nearly edge-on system with $\cos \iota \sim 0$, the relative error bar of $g(m)$ is about 3/5 of that of A , as a consequence of $g(m) \propto A^{3/5}$, except for when $\text{SNR}(\text{gibmcmc}) \leq 3$. For a nearly face-on system, the relative error bar of A is much larger than that of $g(m)$, as a consequence of the strong degeneracy between A and $\cos \iota$ (see Fig. 2).

Deviation from the simple power-law relation is anticipated at low SNR, leading to a more stringent upper bound $\delta_{gm,max}$ and a less restrictive lower bound $\delta_{gm,min}$. This outcome is a

consequence of the log-uniform distribution of the prior for parameter A .

For such low SNR systems, noise can significantly distort or completely obscure the power-law relation, highlighting a limitation that requires further investigation. Additionally, this relation assumes prior knowledge of the system's orbital frequency, distance, and sky location; when these parameters are subject to measurement uncertainty, non-trivial modifications to the relation Eq. 11 are expected. Given the faintness of the WD, distance is likely the limiting factor. Fortunately, its effect on the GW mass function error takes a simple form, as discussed in Appendix A. The impact of uncertainty in sky location and orbital frequency could be much more complicated, and we look forward to future study addressing this issue. Overall, the empirical relation in Eq. 11 provides a straightforward way to estimate the accuracy of the GW mass function achievable with LISA observations, bypassing the need for mock parameter estimation.

3. RESULTS

3.1. Analytical estimates of NS's mass by two mass functions

As both optical observations and analysis of GW detection indicated, the main issue for binary parameter estimation is the undetermined mass-inclination degeneracy. For a binary system with both optical observations and GW detection, both mass functions can be measured, each subject to an error bar. As we have assumed that the companion mass m_c is known, the maximum mass can be calculated by solving

$$\begin{cases} f(m)_{\max} = \frac{(m_{ns,\max})^3 \sin^3 \iota}{(m_{ns,\max} + m_c)^2}; \\ g(m)_{\max} = \frac{(m_{ns,\max} m_c)^{3/5}}{(m_{ns,\max} + m_c)^{1/5}} \left[\cos^2 \iota + \left(\frac{1 + \cos^2 \iota}{2} \right)^2 \right]^{3/10} \end{cases} \quad (12)$$

simultaneously, and similarly for the minimum mass. In addition to the joint constraint, the binary mass function places a lower bound of m_{ns} via

$$\frac{(m_{ns,\min})^3}{(m_{ns,\min} + m_c)^2} \geq f(m)_{\min}. \quad (13)$$

For an edge-on system, the variation of radial velocity is the maximum, leading to a stringent lower bound of the mass. The GW mass function alone also provides an upper bound

$$\frac{(m_{ns,\max} m_c)^{3/5}}{(m_{ns,\max} + m_c)^{1/5}} \leq 2^{3/5} g(m)_{\max}, \quad (14)$$

that is only relevant for high SNR systems that are close to an edge-on configuration. For a face-on system, we have $f(m)_{\min} \approx 0$, and the lower bound is trivial.

Using the empirical relation Eq. 11 the minimum GW SNR required to achieve a measurement of (at least) $m_{ns} = (2 \pm 0.2) M_\odot$ at 90% confidence level is shown in Fig. 4.

When $f(m)$ is measured accurately with $\delta_{\text{fm}} \lesssim 10\%$, the minimum SNR required to probe m_{NS} with the same precision is smaller for nearly edge-on systems. If the binary mass function is measured with $\pm 5\%$ accuracy or smaller, even systems with $\text{SNR} \lesssim 10$ can constrain NS mass within $\pm 0.2 M_{\odot}$ for optimal system configuration. The lower bound, which is particularly important for constraining NS internal structure, is usually better than $0.2 M_{\odot}$ for nearly edge-on systems, primarily due to the constraint imposed by $f(m)_{\text{min}}$ alone. For nearly face-on systems, the lower bound of the binary mass function $f(m)$ vanishes, and the joint constraint depends mainly on the GW observations. With such precise binary mass function measurements, NS-WD binaries with $\text{SNR} \geq 25$ can determine the mass to within $\pm 0.2 M_{\odot}$, regardless of other orbital parameters. When the binary mass function is measured less accurately with $\delta_{\text{fm}} \geq 10\%$, the preference for inclination angle is reversed. For nearly edge-on configuration, the constraint is primarily determined by $f(m)$. Therefore, when $f(m)$ is measured with large uncertainty, even a perfect measurement of $g(m)$ is insufficient to constrain m_{NS} to within $\pm 0.2 M_{\odot}$. However, it should be noted that if such a system has a sufficiently high SNR, the $A - \cos \iota$ degeneracy disappears (see e.g., Fig. 6), and the constraint from GW observations alone could be better than $\pm 0.2 M_{\odot}$. This is not captured by Fig. 6, which is calculated using the GW mass function via Eq. 11.

Interestingly, the minimum SNR for binaries with a heavier companion is smaller than that for a lighter companion. This dependence becomes prominent when $f(m)$ is measured with a 10% error, in which case the minimum SNR for a heavy companion is approximately half that of a lighter companion. As NS-WD binaries with heavier WD has larger GW amplitude, this suggests that accurate NS mass measurement prospects lie in such heavy NS-WD binaries. Using Eq. 4, the minimum GW SNR can be translated into a relation between maximum binary distance and orbital period. The result is shown in Fig. 5, in which we adopt $\delta_{\text{fm}} = 5\%$, 20% and $\delta_{\text{gm},90\%}$. Due to the dependency of SNR and minimum SNR on m_c , the probing distance for NS-WD binaries with a heavier companion of $m_c = 0.6 M_{\odot}$ is about ten times larger than that for a lighter companion with $m_c = 0.1 M_{\odot}$. Assuming a median distance of 10 kpc, NS-WD binaries with $P_{\text{orb}} \lesssim 30$ min and a heavy companion (i.e. $m_c \gtrsim 0.6 M_{\odot}$) are the more promising candidates for probing NS mass.

The generic results to Eq. 12 is complicated in form, and for the ease of computation, we present an approximate formula in Appendix A. The formula is applicable when the relative errors of all quantities are much smaller than unity. Supplemented by the empirical relation outlined in Eq. 11, the approximate formula can be employed to estimate the joint constraint on the NS mass for NS-WD binaries with multi-messenger method.

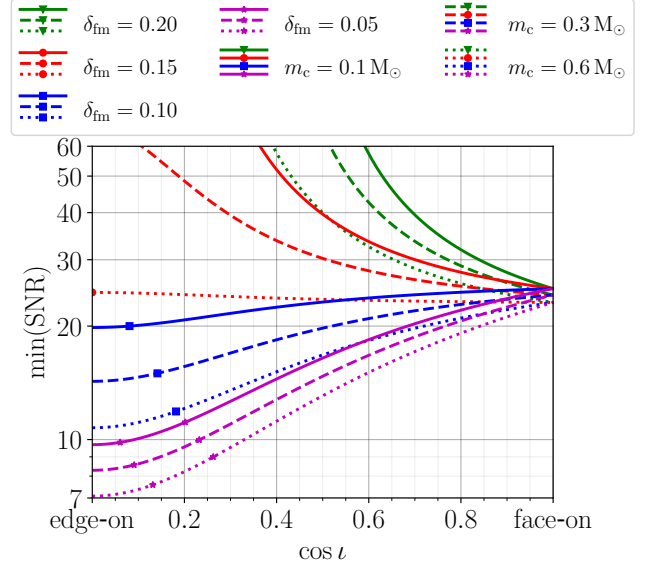


Figure 4. The minimum SNR of the NS-WD binaries required to achieve an measurement of $m_{\text{NS}} = (2 \pm 0.2) M_{\odot}$ for different companion masses and different measurement accuracy of δ_{fm} . The marker(s) on each line represent the value of $\cos \iota$, below which the lower bound of m_{NS} placed by $f(m)_{\text{min}}$ alone is equivalent or better than $1.8 M_{\odot}$. From right to left, the lower bound due to $f(m)_{\text{min}}$ alone is 1.8 and 1.9 M_{\odot} . For some lines, some markers on the left are missing when their best constraints can not reach 1.9 M_{\odot} level.

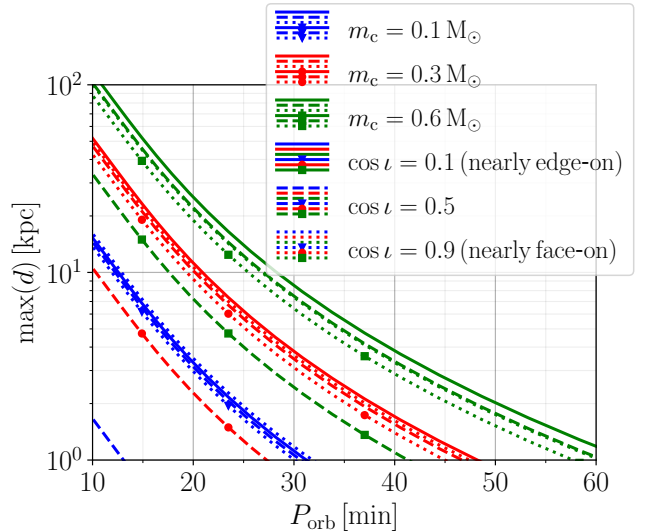


Figure 5. The maximum distance of the NS-WD binary for probing a measurement of $m_{\text{NS}} = 2 \pm 0.2 M_{\odot}$. The unmarked lines represent cases with $\delta_{\text{fm}} = 5\%$ and the marked lines represent cases with $\delta_{\text{fm}} = 20\%$. It is important to highlight that, for cases with $\cos \iota = 0.1$ and $\delta_{\text{fm}} = 5\%$, the lower bound exceeds $1.8 M_{\odot}$.

3.2. The joint constraints on the NS's mass

The degeneracy between the GW amplitude A and inclination angle translates into a degeneracy between m_{NS} and $\cos \iota$. Fig. 6 illustrates such mass-inclination degeneracy from GW

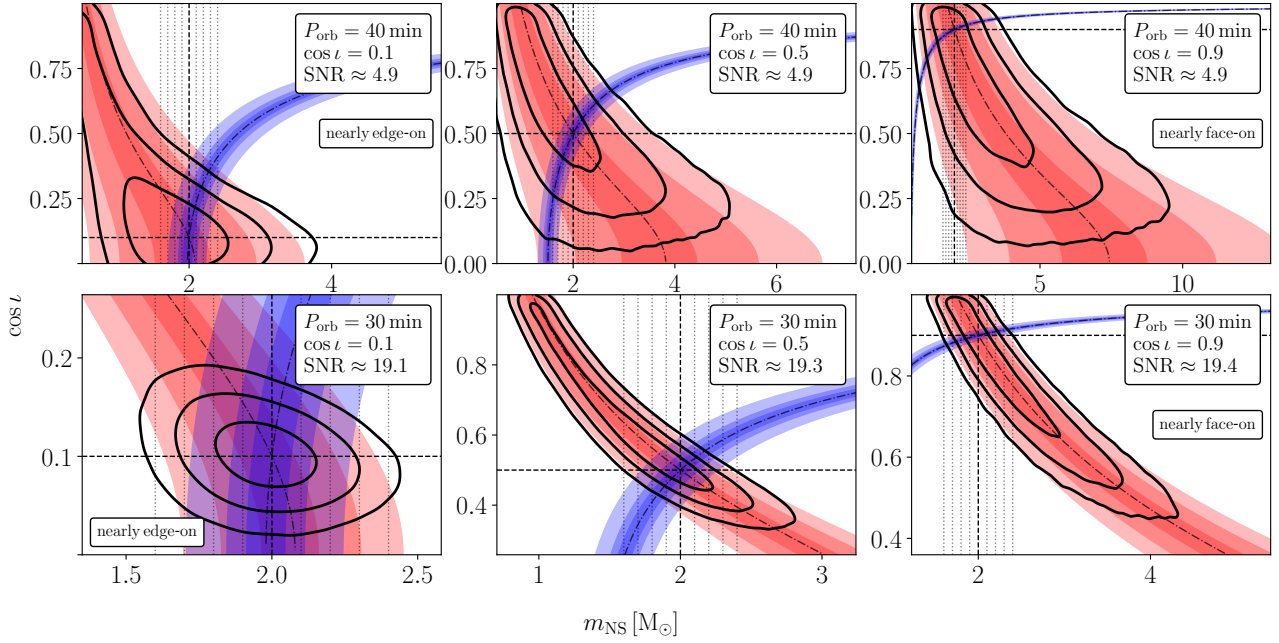


Figure 6. The constraints on the binary parameters for 6 different binary systems with $m_{\text{ns}} = 2 M_{\odot}$ and $m_c = 0.6 M_{\odot}$ located at (top left to right) $d = 5.22, 8.11, 12.94$ kpc and (bottom left to right) $d = 2.99, 4.65, 7.41$ kpc. In each panel, the red strips (that extends from top left to bottom right) represent the 50%, 90% and 99% confidence intervals of the GW mass function $g(m)$ (similar to the shaded region in the last panel of Fig. 2). The blue strips (that extends from bottom left to top right) represent the $\pm 5\%$, 10% and $\pm 20\%$ error bars of the binary mass function $f(m)$. The black contours represent 2-dimensional confidence intervals of 50%, 90% and 99%. The dash-dotted lines represent the true value of $f(m)$ and $g(m)$. The horizontal and vertical dashed lines represent the true values of m_{ns} and $\cos \iota$ -s. The vertical dotted lines are reference lines of $m_{\text{ns}} = 1.6 - 2.4 M_{\odot}$ with $0.1 M_{\odot}$ spacing.

and also EM observations for a few NS-WD binaries with $\text{SNR} \approx 5$ and ≈ 20 . The two almost-diagonal strips represent the mass functions $f(m)$ and $g(m)$, respectively. The black contours represent the 50%, 90%, and 99% confidence intervals of 2D PDF of $\cos \iota - m_{\text{ns}}$. In the following, we will refer to the intersection of $f(m)$ and $g(m)$ strips as $g(m) - f(m)$ constrain and the intersection of $f(m)$ strip and 2D contour of $\cos \iota - m_{\text{ns}}$ from `gbmcmc` simulation as $2D - f(m)$ constrain.

The first column of Fig. 6 represent the nearly edge-on cases when the lower bound of m_{ns} from $f(m)_{\text{min}}$ alone outstands (or is comparable to) the joint constraint from the multi-messenger method. The upper panel of the first column shows the parameter estimates of a binary system consisting of a $2 M_{\odot}$ NS and a companion star of $m_c = 0.6 M_{\odot}$ revolving around each other with $P_{\text{orb}} = 40$ min at a distance of 5.22 kpc, and viewed at an inclination $\cos \iota = 0.1$. The system has $\text{SNR} \approx 5$. When $f(m)$ is measured with $\pm 1\%$, the $m_{\text{ns}} < 1.97 M_{\odot}$ and $m_{\text{ns}} > 2.17 M_{\odot}$ can be ruled out at 90% confidence interval for $2D - f(m)$ constrain. At 50% confidence interval, the mass is constrained to be $1.97 - 2.08 M_{\odot}$. For a similarly edge-on system with $\text{SNR} \approx 20$ (lower left panel of Fig. 6), δ_{gm} is approximately a quarter of the value in the previous case. Consequently, the upper bound of m_{ns} from $2D - f(m)$ constrain is $2.03 M_{\odot}$ at 50% confidence interval and $2.04 M_{\odot}$ at 90% confidence interval which are also about

a quarter of the values in the previous case. Comparing these two cases reveals that the apparent mass-inclination degeneracy from GW observation is evident for edge-on systems at lower SNR, as indicated by the elongated shape of the black contour and its alignment with $g(m)$ strips. Such degeneracy is absent in the case of edge-on binary at higher SNR, in which case the GW mass function becomes redundant and the NS mass can be determined solely from the GW observations. Regarding the constraints on m_{ns} , the results obtained from $g(m) - f(m)$ constrain slightly underestimate the actual constraints derived from the joint GW and EM observations.

The second column of Fig. 6 represents cases with intermediate inclination angle $\cos \iota = 0.5$. The upper middle panel of Fig. 6 shows a system with $\text{SNR} \approx 5$. If $f(m)$ is measured with an error bar $\pm 1\%$, $m_{\text{ns}} < 1.6 M_{\odot}$ and $m_{\text{ns}} > 2.5 M_{\odot}$ can be ruled out by both $g(m) - f(m)$ and $2D - f(m)$ at 90% confidence level. For the lower middle panel of Fig. 6, the SNR is approximately four times the previous case, and the corresponding constraints are $1.88 - 2.10 M_{\odot}$ for $g(m) - f(m)$ and $1.88 - 2.12 M_{\odot}$ for $2D - f(m)$, respectively, when $\delta_{\text{fm}} = 1\%$. The mass-inclination degeneracy from GW observation persists for both cases, with $g(m)$ contour aligning nicely with the $m_{\text{NS}} - \cos \iota$ contour for $\text{SNR} \approx 5$ case, and a slight mismatch for $\text{SNR} \approx 10$ case at small m_{NS} , which are reminiscent of the first panel of this figure. In fact, the mass-inclination

degeneracy gradually eases when $\text{SNR} \gtrsim 15$, and further disappear when $\text{SNR} \gtrsim 40$.

The third column represents nearly face-on NS-WD binaries with $\cos \iota = 0.9$. For the $\text{SNR} \sim 5$ case, the 90% constraints on m_{NS} from $2\text{D} - f(m)$ is about $\pm 1 M_{\odot}$. In contrast, for the case with $\text{SNR} \sim 20$, the constraint narrows to around $\pm 0.24 M_{\odot}$, and remains insensitive to the value of δ_{fm} . Both constraints are much worse than those of intermediate inclination angles and near $\pi/2$ inclination angles at same SNR. For these nearly face-on systems, the mass-inclination degeneracy persists even for system with large SNR, which is evident from Fig. 2. In fact, within the parameter space considered in this work, this degeneracy consistently persist for all systems with $\text{SNR} \leq 400$, implying its relevance for any realistic GW sources detectable by LISA. For the selected 6 systems, nearly edge-on systems ($\cos \iota = 0.1$) have tighter constraints on m_{NS} compared to nearly face-on systems ($\cos \iota = 0.9$) when the GW strength is comparable.

Similar parameter estimations were performed for a larger set of binaries with the same $m_{\text{NS}} = 2 M_{\odot}$, $m_{\text{c}} = 0.6 M_{\odot}$, with different orbital periods $P_{\text{orb}} = 20 - 60$ min located at $d = 1 - 12$ kpc away, with an inclination angle ranging from $\cos \iota = 0.1$ to $\cos \iota = 0.9$. The joint constraints on the NS mass are shown in Fig. 7. For systems with SNR smaller than the reference SNR, $\delta_{\text{gm}} \geq \delta_{\text{fm}}$. In which case, the error bar δ_m is dominated by the uncertainty in GW observation. Consequently, as explained in the previous section, error bars for nearly edge-on systems are slightly smaller compared to nearly face-on systems for the same orbital parameters, despite having a slightly larger SNR. The $g(m) - f(m)$ constraints (blue triangles) align with the joint constraints of $2\text{D} - f(m)$ (red circles), particularly for systems with small SNR. In this regime, the GW mass function captures the essence of the mass-inclination degeneracy, accurately reproducing and improving upon the joint constraints from multi-messenger observations.

For systems with SNR much larger than the reference SNR, $\delta_{\text{gm}} \ll \delta_{\text{fm}}$, the GW amplitudes of the binary systems are sufficiently large, such that the constraints on NS mass is dominated by the uncertainty of the binary mass function $f(m)$. In this regime, constraints on m_{NS} for edge-on systems outperform those for face-on systems. Significant discrepancy arises between $g(m) - f(m)$ constraint and $2\text{D} - f(m)$ constraint for system with $\cos \iota \leq 0.5$ and $\text{SNR} \geq 100$, where the mass-inclination degeneracy has completely eased, as shown in the middle and right panels at large SNR in Fig. 7.

The lower bounds of m_{NS} for system with $\cos \iota \sim 0$ are much better than their upper bounds. This is due to the stringent constraint from $f(m)_{\text{min}}$ alone. When the error bars are much smaller than unity, the lower bounds are approximately $m_{\text{NS}} \geq 2 M_{\odot} \times \sin^3 \iota$.

As demonstrated by the systems discussed in this section, the mass constraints derived from the intersection of $g(m) - f(m)$ align closely with those obtained from the intersection of $2\text{D} - f(m)$ for NS-WD binaries with $\text{SNR} \lesssim 100$. Moreover, the former is accurately described by Eq. 12 and the empirical relation Eq. 11. We can therefore conclude that the proposed analytical formula for δ_{gm} , despite being an empirical relation, is well-suited for estimating mass constraints for NS-WD systems across a broad parameter range.

4. DISCUSSIONS

4.1. GW mass-inclination degeneracy

As pointed out in the previous section, the degeneracy between mass and inclination angle is prominent in systems with low SNR and it is reduced when SNR increases. For nearly edge-on systems with $\cos \iota = 0.1$, the degeneracy would become less severe when $\text{SNR} \gtrsim 20$; for systems with an intermediate inclination of $\cos \iota = 0.5$, the degeneracy diminishes when $\text{SNR} \gtrsim 40$. However, for nearly face-on systems with $\cos \iota = 0.9$, the degeneracy persists until $\text{SNR} \sim 400$.

The origin of this degeneracy lies in the indistinguishability of the two polarization modes, h_+ and h_{\times} , which depends on both the SNR of the GW signal and the relative strength of the two modes. It is reminiscent of the distance-inclination degeneracy observed in the analysis of compact object binaries detected by the LIGO-Virgo-KAGRA (LVK) Scientific Collaboration network, which have been studied systematically by Usman et al. (2019). These two degeneracies both stem from the degeneracy between GW amplitude and inclination angle (the $A - \iota$ degeneracy), albeit with subtle differences.

The $A - \iota$ degeneracy can be illustrated with the following example. Consider two L-shaped detectors orientated with a 45° offset, with $\psi = 0$ set to correspond to the configuration where the two detectors align with h_+ and h_{\times} respectively. For an exact face-on binary system with an arbitrary polarization angle, the signals recorded in both detectors are identical to those of a closer (or more massive) exact edge-on system with $\psi = \pi/8$ (or $3\pi/8$, etc), with the exception of a phase difference. An exact edge-on system with polarization angle slightly deviating from $\pi/8$ would therefore resemble a nearly face-on system with an arbitrary polarization angle. In Bayesian inference, the range of each parameter is determined by marginalizing over the remaining parameters. Consequently, a nearly edge-on system is prone to being misconstrued as a nearly face-on system, whereas the reverse is not necessarily true. The relative strength of two polarization modes $h_{\times}/h_+ \gtrsim 94\%$ for $\cos \iota \geq 0.7$, suggesting that the GW signal from nearly face-on systems become nearly indistinguishable from one another. This example elucidates the prominent degeneracy observed in Fig. 2, and the $\cos \iota = 0.5$ and $\cos \iota = 0.9$ cases shown in Fig. 6. Examining the system presented in Fig. 2, where the injection parameter is

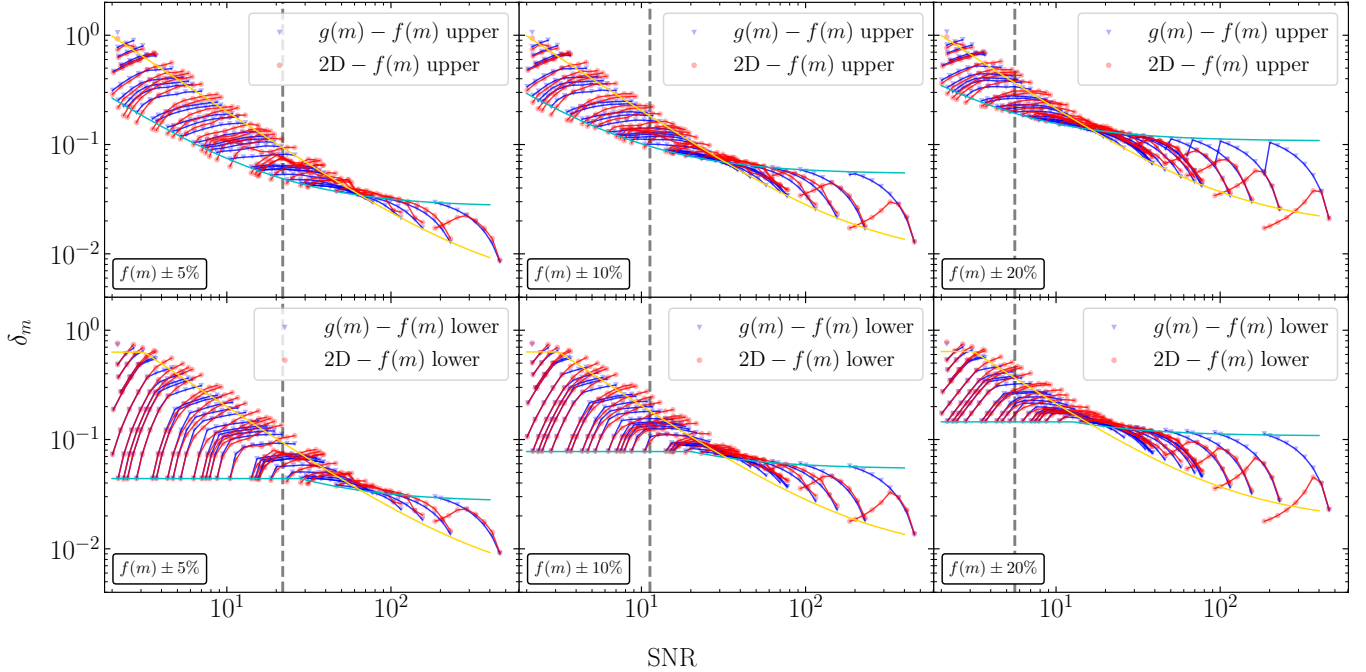


Figure 7. The relative size of the error bar of m_{ns} versus the SNR of a wide range of NS-WD binaries with $P_{\text{orb}} = 20 - 60$ min, $\cos i = 0.1 - 0.9$ and $d = 1 - 12$ kpc. The upper panels show the upper bound $\delta_m \equiv (m_{\text{ns,max}} - m_{\text{ns,0}})/m_{\text{ns,0}}$, and the lower panels show the lower bound $\delta_m \equiv (m_{\text{ns,0}} - m_{\text{ns,min}})/m_{\text{ns,0}}$. The $g(m) - f(m)$ and $2\text{D} - f(m)$ constraints are calculated by finding the intersection of 90% confidence intervals of 1D PDF of $g(m)$ and that of 2D PDF of $\cos i - m_{\text{NS}}$ with $f(m) \pm \delta_{\text{fm}}$, assuming $\delta_{\text{fm}} = 5\% - 20\%$. The vertical dashed lines represent the reference SNRs when $\delta_{\text{gm}} \approx \delta_{\text{fm}}$, and we have $\delta_{\text{gm}} \leq \delta_{\text{fm}}$ on the left-hand side of the dashed line. Systems of the same orbital period and distance, but with different inclination angles are connected with solid lines, with nearly edge-on system (i.e. $\cos i = 0.1$) on the left end and nearly face-on system $\cos i = 0.9$ on the right end. The cyan (yellow) line in each panel represents the reference line calculated using Eq. A2 and Eq. 11 for $\cos i = 0.1$ (0.9). As depicted in the figure, these reference lines distinctly trace the dependence of δ_m on SNR for systems with the respective inclination angles. The turning of the blue curve in the top-right panel for high SNR systems is due to the constraint imposed by $g(m)$ alone (Eq. 14).

$\cos i = 0.9$, the marginalized posterior of $\cos i$ extends towards both smaller and larger values, favoring $\cos i = 1$, as an exact face-on template provides a decent fit to the signal, regardless of the polarization angle.

For a nearly edge-on binary system, the degeneracy is reduced quickly as SNR increases, and it disappears when $\text{SNR} \gtrsim 20$, a phenomenon also observed in LVK binaries. In LVK observations, when the the network of GW detectors is equally sensitive to both polarization modes, the signals recorded in both detectors are dominated by the h_+ mode (unless when ψ is very close to 0 or $\pi/4$). The relative strength of the two signals provides additional information about the polarization angle, which will aid in resolving the $A - i$ degeneracy. To be more precise, this measurement constrains $\phi - 2\psi$, as demonstrated in Fig. 2⁴.

⁴The case presented here is nearly face-on, but this particular feature also exists for nearly edge-on systems with low SNR. A similar degeneracy was discussed by Usman et al. (2019), although it was reported as $\phi \pm \psi$. Our additional factor of 2 is likely due to a difference in the convention of the polarization angle.

In the case of Galactic binaries, the situation is somewhat more intricate. Unlike the binaries observed by LVK network, where the length of the GW signal is comparable to the binary orbital period (which allows for a precise estimation of ϕ) the observational time needed for the declaration of a detection is significantly longer than their orbital period for Galactic binaries. In the latter scenario, information about the initial orbital phase ϕ is lost, rendering it as a free orbital parameter. Due to the strong degeneracy between ψ and ϕ , ψ also becomes unconstrained. The upper panels of Fig. 6 illustrate such cases. Regardless of true inclination angle of the system, face-on templates almost always provide a decent fit to the signal, suggesting that the parameter estimation results tend to favor, or at least are consistent with larger values of $\cos i$.

For systems with higher SNRs, the situation differs. As LISA rotates in space, the polarization angle varies with respect to the detector's rest frame. Consequently, each TDI channel experiences at least one episode of high GW signal when its orientation aligns exactly with h_+ and one episode of low GW signal when its orientation aligns with h_\times . This distinctive observational feature is absent in the low SNR

cases due to difficult of signals being entangled with noise. Such feature enables us to differentiate the amplitude of two polarization modes, thereby constraining the system's inclination angle. This condition corresponds to the cases in the bottom-left panel of Fig. 6.

4.2. Formation channels of compact NS-WD binaries

Despite the prevalent belief (Tauris 2018; Korol et al. 2024; He et al. 2024) that compact NS-WD systems that are observable with LISA could exist, there is no confirmed observation of such systems. Instead, the observed NS-WD binaries are typically found in much wider orbits⁵. Therefore, it is worth discussing the possible formation channels for the specific binary systems of interest. NS-WD binaries are evolutionary end points of LMXB/IMXB, and a correlation between the post-LMXB orbital period and the WD mass is expected (see Rappaport et al. 1995; Tauris & Savonije 1999; Istrate et al. 2014), where systems with lighter WDs tend to have closer orbits. The post-LMXB/post-IMXB evolution is driven mainly by the loss of orbital angular momentum through gravitational radiation (see e.g. Paczyński 1971), which constrains that the initial orbital period of the binary has to be $\lesssim 12$ hr in order for it to reach the LISA sensitivity band within a Hubble time. This narrow range of initial orbital period and the correlation of orbital period with WD mass at the end of LMXB/IMXB phase suggests that only those with WD mass smaller than $\lesssim 0.2 M_{\odot}$ can evolve towards this compactness that is relevant for GW observation (Tauris 2018), although the exact WD-mass threshold depends on the mass and metallicity of the progenitor, the efficiency of magnetic braking mechanism and the initial orbital period in the pre-LMXB/pre-IMXB phase (see e.g. Tauris & Savonije 1999; Chen et al. 2020, 2021).

Alternatively, the NS may form after the WD when the two progenitor stars in the initial binaries are massive enough (Tutukov & Yungel'Son 1993). This formation scenario was proposed to explain the origin of PSR B2303+46 and PSR J1141–6545 (Tauris & Sennels 2000), and the resulting binary favors more massive WD, i.e. CO or ONeMg WD.

In dense nuclear stellar cluster or globular cluster where the stellar population is old, the terminating orbital period of the LMXB phase would be about a factor of two shorter than those in the field (Rappaport et al. 1995). Moreover, the dense stellar environment underscores the significance of dynamical interactions. Compact NS-WD binaries might be produced through dynamical capture, three-body interactions, or even four-body interactions. Consider a binary with

binding energy

$$E_b = \frac{G m_{\text{ns}}^2 q}{2a} = \frac{G^{2/3}}{2} \left(\frac{2\pi}{P_{\text{orb}}} \right)^{2/3} m_{\text{ns}}^{5/3} \left[\frac{q}{(1+q)^{1/3}} \right], \quad (15)$$

where $q = m_2/m_{\text{ns}}$, The hardening rate of it is roughly

$$\frac{dE_b}{dt} \approx \xi G^2 \left(\frac{n_* \bar{m}^3}{\langle \sigma \rangle} \right) \quad (16)$$

(Heggie 1975), where $\xi \sim 10$, which includes contributions to binary hardening via wide/close three-body encounters, exchange and resonant encounter⁶. \bar{m} represent the averaged mass of the encounters, n_* represents the stellar number density and $\langle \sigma \rangle$ represents the velocity dispersion. The time scale it takes for a NS-WD binary to harden till the region where GW dominates (i.e. when $P_{\text{orb}} \sim$ days) is approximately (assuming $q = 0.4$):

$$T_{\text{harden}} = \frac{m_{\text{ns}}^{5/3}}{2\xi G^{4/3}} \frac{\langle \sigma \rangle}{n_* \bar{m}^3} \left(\frac{2\pi}{P_{\text{orb}}} \right)^{2/3} \frac{q}{(1+q)^{1/3}} \approx 26 \text{ Gyr} \left(\frac{m_{\text{ns}}}{2 M_{\odot}} \right)^{5/3} \left(\frac{10}{\xi} \right) \left(\frac{\langle \sigma \rangle}{200 \text{ km s}^{-1}} \right) \times \left(\frac{12 \text{ hr}}{P_{\text{orb}}} \right)^{2/3} \left(\frac{10^6 \text{ pc}^{-3}}{n_*} \right) \left(\frac{1 M_{\odot}}{\bar{m}} \right)^3, \quad (17)$$

which is about double the Hubble time. We have adopted a stellar density of $10^6 M_{\odot} \text{ pc}^{-3}$ at the inner 1 pc (Merritt 2010) of Galactic Centre, and a stellar velocity dispersion of 200 km s^{-1} . Similarly, for a typical globular cluster with core stellar density of $\sim 10^4 M_{\odot} \text{ pc}^{-3}$ (Carballo-Bello et al. 2012; Pancino et al. 2017) and velocity dispersion of $\sim 5 \text{ km s}^{-1}$ (see e.g. de Boer et al. 2019), the time scale for hardening is about 5 times the Hubble time⁷. The hardening due to stellar encounters and subsequent GW radiation would therefore be sufficient to produce the target NS-WD binaries if the binaries start off sufficiently hard themselves. Note that this hardening formula has included three-body exchange and resonant encounters, both of which tend to eject the least massive star among the triples. This process would likely produce NS-WD binary with a heavier WD, the gravitational radiation for which is more efficient.

⁶ We have dropped the dependency of the results on the mass ratio for simplicity, given that all the masses considered here are on the order of unity.

⁷ In the calculations we set $\bar{m}/M_{\odot} = 1$, but stars in the Nuclear Star Cluster of the Galactic Centre (see Chen et al. 2023) and in globular clusters are old stars with mass well below $1 M_{\odot}$. Using a more accurate value for \bar{m}/M_{\odot} , however, would not alter the conclusion that hardening would take much longer than the Hubble time.

⁵ An up-to-date list of observed NS-WD binaries is available in the ATNF catalog: <https://www.atnf.csiro.au/research/pulsar/psrcat>

5. CONCLUSIONS

Compact NS-WD binaries potentially hold the most massive NSs. Measuring their masses is essential for our understanding of the densest matter in our Universe. In this work, we studied the potential of using GW observation to measure the parameters of NS-WD binary and proposed a novel multi-messenger method to constrain NS masses in these systems by combining the GW and EM detections. For a series of hypothetical NS-WD binaries with sub-hourly orbital period inside our Galaxy, we generated 4 years of mock GW data for each system and performed parameter estimation using the `gbmcmc` package. By combining the GW information with the binary mass function from EM observation, the degeneracy between mass and inclination angle can be resolved, allowing for much tighter constraints on the NS mass. We showed that for our multi-messenger method, the major factors that determine the constraint of the NS mass are the GW SNR of the NS-WD binary, the accuracy of the binary mass function, and the inclination angle. In general, for a realistic range of SNR (i.e. ≤ 100), edge-on systems are favored over face-on systems in terms of parameter estimation.

Regardless of the inclination of the systems, our method suggests that the m_{ns} of a NS-WD binary can be constrained to within $\pm 0.2 M_{\odot}$ as long as their SNR ≥ 25 , and the binary mass function is measured within $\pm 10\%$ accuracy. For a NS-WD binary with $P_{\text{orb}} \sim 60$ min and $m_c = 0.6 M_{\odot}$, the system needs to be within ~ 1 kpc. However, for a system with $P_{\text{orb}} \sim 20$ min, the distance threshold for the acceptable mass determination is about ~ 20 kpc. Our study suggests that those NS-WD binaries in globular clusters and in our Galaxy can be used to constrain the mass of massive NS.

Last but not least, we defined a new concept: GW mass function $g(m)$, which is derived from GW observations, in

contrast to the binary mass function derived from optical photometric or spectroscopy observations. We showed that the error bar of the GW mass function follows a simple power law relation with the GW SNR of NS-WD binaries, regardless of the companion's mass, the orbital period, or the viewing inclination, validating the universality of this definition. Moreover, the GW mass function captures the essence of the mass-inclination angle degeneracy in GW observations, and therefore, serves as a handy tool for constraining m_{ns} with multi-messenger observations.

ACKNOWLEDGEMENTS

We thank the anonymous referee of a previous paper of ours for encouraging us to fully develop the conceptual framework of the GW mass function. We thank Silvia Zane for the discussions on mass-radius relations of NSs and various tests in future X-ray studies, Daisuke Kawata on stellar populations and density at the Galactic Centre, and Qin Han on the evolution of compact binaries. We also thank Jane Yap, Joana Teixeira and Jun Lau for general discussions and comments on this work. KW thanks the hospitality of NTHU IoA, where a substantial part of this work was conducted, during his visits. KJL is supported by a PhD Scholarship from the Vinson and Cissy Chu Foundation and by a UCL MAPS Dean's Prize. KW and JSL acknowledge the support of the UCL Cosmoparticle Initiative. This work is supported by the National Science and Technology Council of Taiwan (ROC) under the grants 110-2628-M-007-005 and 112-2112-M-007-042 (PI: A. Kong). This work has made use of the NASA Astrophysics Data System.

Software: GetDist (Lewis 2019), Astropy (Astropy Collaboration et al. 2022b), `gbmcmc` (Littenberg et al. 2020a), Mathematica (Wolfram Research, Inc. 2024)

REFERENCES

- Akmal, A., Pandharipande, V. R., & Ravenhall, D. G. 1998a, *PhRvC*, 58, 1804, doi: [10.1103/PhysRevC.58.1804](https://doi.org/10.1103/PhysRevC.58.1804)
- . 1998b, *PhRvC*, 58, 1804, doi: [10.1103/PhysRevC.58.1804](https://doi.org/10.1103/PhysRevC.58.1804)
- Alford, M. G., Han, S., & Prakash, M. 2013, *PhRvD*, 88, 083013, doi: [10.1103/PhysRevD.88.083013](https://doi.org/10.1103/PhysRevD.88.083013)
- Althaus, L. G., García-Berro, E., Isern, J., & Córscico, A. H. 2005, *A&A*, 441, 689, doi: [10.1051/0004-6361:20052996](https://doi.org/10.1051/0004-6361:20052996)
- Amaro-Seoane, P., Audley, H., Babak, S., et al. 2017, arXiv e-prints, arXiv:1702.00786. <https://arxiv.org/abs/1702.00786>
- Antoniadis, J., Freire, P. C. C., Wex, N., et al. 2013, *Science*, 340, 448, doi: [10.1126/science.1233232](https://doi.org/10.1126/science.1233232)
- Astropy Collaboration, Price-Whelan, A. M., Lim, P. L., et al. 2022a, *ApJ*, 935, 167, doi: [10.3847/1538-4357/ac7c74](https://doi.org/10.3847/1538-4357/ac7c74)
- . 2022b, *ApJ*, 935, 167, doi: [10.3847/1538-4357/ac7c74](https://doi.org/10.3847/1538-4357/ac7c74)
- Avancini, S. S., Menezes, D. P., Alloy, M. D., et al. 2008, *PhRvC*, 78, 015802, doi: [10.1103/PhysRevC.78.015802](https://doi.org/10.1103/PhysRevC.78.015802)
- Baldo, M., Burgio, G. F., & Schulze, H. J. 2000, *PhRvC*, 61, 055801, doi: [10.1103/PhysRevC.61.055801](https://doi.org/10.1103/PhysRevC.61.055801)
- Barstow, M. A., Holberg, J. B., Hubeny, I., et al. 2001, *MNRAS*, 328, 211, doi: [10.1046/j.1365-8711.2001.04855.x](https://doi.org/10.1046/j.1365-8711.2001.04855.x)
- Baym, G., Hatsuda, T., Kojo, T., et al. 2018, *Reports on Progress in Physics*, 81, 056902, doi: [10.1088/1361-6633/aaae14](https://doi.org/10.1088/1361-6633/aaae14)
- Bédard, A., Bergeron, P., & Fontaine, G. 2017, *ApJ*, 848, 11, doi: [10.3847/1538-4357/aa8bb6](https://doi.org/10.3847/1538-4357/aa8bb6)
- Benacquista, M. J., Portegies Zwart, S., & Rasio, F. A. 2001, *Classical and Quantum Gravity*, 18, 4025, doi: [10.1088/0264-9381/18/19/308](https://doi.org/10.1088/0264-9381/18/19/308)
- Bergeron, P., Saffer, R. A., & Liebert, J. 1992, *ApJ*, 394, 228, doi: [10.1086/171575](https://doi.org/10.1086/171575)

- Bradley, P. A., & Winget, D. E. 1994, *ApJ*, 430, 850, doi: [10.1086/174456](https://doi.org/10.1086/174456)
- Bragaglia, A., Renzini, A., & Bergeron, P. 1995, *ApJ*, 443, 735, doi: [10.1086/175564](https://doi.org/10.1086/175564)
- Burdge, K. B., Coughlin, M. W., Fuller, J., et al. 2019a, *Nature*, 571, 528, doi: [10.1038/s41586-019-1403-0](https://doi.org/10.1038/s41586-019-1403-0)
- . 2019b, *Nature*, 571, 528, doi: [10.1038/s41586-019-1403-0](https://doi.org/10.1038/s41586-019-1403-0)
- Burdge, K. B., Prince, T. A., Fuller, J., et al. 2020, *ApJ*, 905, 32, doi: [10.3847/1538-4357/abc261](https://doi.org/10.3847/1538-4357/abc261)
- Carballo-Bello, J. A., Gieles, M., Sollima, A., et al. 2012, *MNRAS*, 419, 14, doi: [10.1111/j.1365-2966.2011.19663.x](https://doi.org/10.1111/j.1365-2966.2011.19663.x)
- Char, P., & Banik, S. 2014, *PhRvC*, 90, 015801, doi: [10.1103/PhysRevC.90.015801](https://doi.org/10.1103/PhysRevC.90.015801)
- Chen, H.-L., Tauris, T. M., Chen, X., & Han, Z. 2022, *ApJ*, 930, 134, doi: [10.3847/1538-4357/ac6608](https://doi.org/10.3847/1538-4357/ac6608)
- Chen, H.-L., Tauris, T. M., Han, Z., & Chen, X. 2021, *MNRAS*, 503, 3540, doi: [10.1093/mnras/stab670](https://doi.org/10.1093/mnras/stab670)
- Chen, W.-C., Liu, D.-D., & Wang, B. 2020, *ApJL*, 900, L8, doi: [10.3847/2041-8213/abae66](https://doi.org/10.3847/2041-8213/abae66)
- Chen, Z., Do, T., Ghez, A. M., et al. 2023, *ApJ*, 944, 79, doi: [10.3847/1538-4357/aca8ad](https://doi.org/10.3847/1538-4357/aca8ad)
- Cooray, A. 2004, *MNRAS*, 354, 25, doi: [10.1111/j.1365-2966.2004.08152.x](https://doi.org/10.1111/j.1365-2966.2004.08152.x)
- Córsico, A. H., Althaus, L. G., Miller Bertolami, M. M., & Kepler, S. O. 2019, *A&A Rv*, 27, 7, doi: [10.1007/s00159-019-0118-4](https://doi.org/10.1007/s00159-019-0118-4)
- Cromartie, H. T., Fonseca, E., Ransom, S. M., et al. 2020, *Nature Astronomy*, 4, 72, doi: [10.1038/s41550-019-0880-2](https://doi.org/10.1038/s41550-019-0880-2)
- de Boer, T. J. L., Gieles, M., Balbinot, E., et al. 2019, *MNRAS*, 485, 4906, doi: [10.1093/mnras/stz651](https://doi.org/10.1093/mnras/stz651)
- Demorest, P. B., Pennucci, T., Ransom, S. M., Roberts, M. S. E., & Hessels, J. W. T. 2010, *Nature*, 467, 1081, doi: [10.1038/nature09466](https://doi.org/10.1038/nature09466)
- Espino, P. L., & Paschalidis, V. 2019, *PhRvD*, 99, 083017, doi: [10.1103/PhysRevD.99.083017](https://doi.org/10.1103/PhysRevD.99.083017)
- Finch, E., Bartolucci, G., Chucherko, D., et al. 2023, *MNRAS*, 522, 5358, doi: [10.1093/mnras/stad1288](https://doi.org/10.1093/mnras/stad1288)
- Finley, D. S., Koester, D., & Basri, G. 1997, *ApJ*, 488, 375, doi: [10.1086/304668](https://doi.org/10.1086/304668)
- Finn, L. S., & Thorne, K. S. 2000, *PhRvD*, 62, 124021, doi: [10.1103/PhysRevD.62.124021](https://doi.org/10.1103/PhysRevD.62.124021)
- Flanagan, É. É., & Hughes, S. A. 1998, *PhRvD*, 57, 4535, doi: [10.1103/PhysRevD.57.4535](https://doi.org/10.1103/PhysRevD.57.4535)
- Fonseca, E., Cromartie, H. T., Pennucci, T. T., et al. 2021, *ApJL*, 915, L12, doi: [10.3847/2041-8213/ac03b8](https://doi.org/10.3847/2041-8213/ac03b8)
- Genest-Beaulieu, C., & Bergeron, P. 2019, *ApJ*, 871, 169, doi: [10.3847/1538-4357/aafac6](https://doi.org/10.3847/1538-4357/aafac6)
- Ghazanfari Mojarrad, M., & Arabsaeyidi, R. 2016, *International Journal of Modern Physics E*, 25, 1650102, doi: [10.1142/S0218301316501020](https://doi.org/10.1142/S0218301316501020)
- He, J.-G., Shao, Y., Xu, X.-J., & Li, X.-D. 2024, *MNRAS*, 529, 1886, doi: [10.1093/mnras/stae683](https://doi.org/10.1093/mnras/stae683)
- Heggie, D. C. 1975, *MNRAS*, 173, 729, doi: [10.1093/mnras/173.3.729](https://doi.org/10.1093/mnras/173.3.729)
- Holberg, J. B., Wesemael, F., & Basile, J. 1986, *ApJ*, 306, 629, doi: [10.1086/164372](https://doi.org/10.1086/164372)
- Holberg, J. B., Wesemael, F., Wegner, G., & Bruhweiler, F. C. 1985, *ApJ*, 293, 294, doi: [10.1086/163237](https://doi.org/10.1086/163237)
- Istrate, A. G., Tauris, T. M., & Langer, N. 2014, *A&A*, 571, A45, doi: [10.1051/0004-6361/201424680](https://doi.org/10.1051/0004-6361/201424680)
- Johnson, P. T., Coughlin, M. W., Hamilton, A., et al. 2023, *MNRAS*, 525, 4121, doi: [10.1093/mnras/stad2579](https://doi.org/10.1093/mnras/stad2579)
- Kawaler, S. D. 1990, in *Astronomical Society of the Pacific Conference Series*, Vol. 11, *Confrontation Between Stellar Pulsation and Evolution*, ed. C. Cacciari & G. Clementini, 494–511
- Kepler, S. O., Koester, D., Romero, A. D., Ourique, G., & Pelisoli, I. 2017, in *Astronomical Society of the Pacific Conference Series*, Vol. 509, *20th European White Dwarf Workshop*, ed. P. E. Tremblay, B. Gaensicke, & T. Marsh, 421, doi: [10.48550/arXiv.1610.00371](https://doi.org/10.48550/arXiv.1610.00371)
- Kilic, M., Brown, W. R., Bédard, A., & Kosakowski, A. 2021, *ApJL*, 918, L14, doi: [10.3847/2041-8213/ac1e2b](https://doi.org/10.3847/2041-8213/ac1e2b)
- Koester, D., Schulz, H., & Weidemann, V. 1979, *A&A*, 76, 262
- Korol, V., Igoshev, A. P., Toonen, S., et al. 2023, *arXiv e-prints*, arXiv:2310.06559, doi: [10.48550/arXiv.2310.06559](https://doi.org/10.48550/arXiv.2310.06559)
- . 2024, *MNRAS*, 530, 844, doi: [10.1093/mnras/stae889](https://doi.org/10.1093/mnras/stae889)
- Korol, V., Rossi, E. M., Groot, P. J., et al. 2017, *MNRAS*, 470, 1894, doi: [10.1093/mnras/stx1285](https://doi.org/10.1093/mnras/stx1285)
- Kupfer, T., Korol, V., Shah, S., et al. 2018, *MNRAS*, 480, 302, doi: [10.1093/mnras/sty1545](https://doi.org/10.1093/mnras/sty1545)
- Kupfer, T., Korol, V., Littenberg, T. B., et al. 2023, *arXiv e-prints*, arXiv:2302.12719, doi: [10.48550/arXiv.2302.12719](https://doi.org/10.48550/arXiv.2302.12719)
- Lattimer, J. M., & Prakash, M. 2004, *Science*, 304, 536, doi: [10.1126/science.1090720](https://doi.org/10.1126/science.1090720)
- . 2007, *PhR*, 442, 109, doi: [10.1016/j.physrep.2007.02.003](https://doi.org/10.1016/j.physrep.2007.02.003)
- . 2010, *arXiv e-prints*, arXiv:1012.3208, doi: [10.48550/arXiv.1012.3208](https://doi.org/10.48550/arXiv.1012.3208)
- Lattimer, J. M., & Swesty, D. F. 1991, *NuPhA*, 535, 331, doi: [10.1016/0375-9474\(91\)90452-C](https://doi.org/10.1016/0375-9474(91)90452-C)
- Lewis, A. 2019, *arXiv e-prints*, arXiv:1910.13970, <https://arxiv.org/abs/1910.13970>
- Li, A., Miao, Z., Han, S., & Zhang, B. 2021, *ApJ*, 913, 27, doi: [10.3847/1538-4357/abf355](https://doi.org/10.3847/1538-4357/abf355)
- Li, Z. H., & Schulze, H. J. 2008, *PhRvC*, 78, 028801, doi: [10.1103/PhysRevC.78.028801](https://doi.org/10.1103/PhysRevC.78.028801)
- Littenberg, T. B., & Cornish, N. J. 2019, *ApJL*, 881, L43, doi: [10.3847/2041-8213/ab385f](https://doi.org/10.3847/2041-8213/ab385f)
- Littenberg, T. B., Cornish, N. J., Lackeos, K., & Robson, T. 2020a, *LDASoft*, free software (GPL), doi: [10.5281/zenodo.2026177](https://doi.org/10.5281/zenodo.2026177)

- . 2020b, *PhRvD*, 101, 123021, doi: [10.1103/PhysRevD.101.123021](https://doi.org/10.1103/PhysRevD.101.123021)
- Maggiore, M. 2008, *Gravitational Waves: Volume 1: Theory and Experiments*, Vol. 1 (Oxford University Press)
- Merritt, D. 2010, *ApJ*, 718, 739, doi: [10.1088/0004-637X/718/2/739](https://doi.org/10.1088/0004-637X/718/2/739)
- Mickaelian, A. M., Mikayelyan, G. A., Abrahamyan, H. V., Paronyan, G. M., & Malkov, O. Y. 2022, *Open Astronomy*, 30, 210, doi: [10.1515/astro-2021-0027](https://doi.org/10.1515/astro-2021-0027)
- Moore, C. J., Cole, R. H., & Berry, C. P. L. 2015, *Classical and Quantum Gravity*, 32, 015014, doi: [10.1088/0264-9381/32/1/015014](https://doi.org/10.1088/0264-9381/32/1/015014)
- Moshfegh, H. R., & Ghazanfari Mojarrad, M. 2013, *European Physical Journal A*, 49, 1, doi: [10.1140/epja/i2013-13001-4](https://doi.org/10.1140/epja/i2013-13001-4)
- Nelemans, G., Yungelson, L. R., & Portegies Zwart, S. F. 2001, *A&A*, 375, 890, doi: [10.1051/0004-6361:20010683](https://doi.org/10.1051/0004-6361:20010683)
- Paczyński, B. 1971, *ARA&A*, 9, 183, doi: [10.1146/annurev.aa.09.090171.001151](https://doi.org/10.1146/annurev.aa.09.090171.001151)
- Pancino, E., Bellazzini, M., Giuffrida, G., & Marinoni, S. 2017, *MNRAS*, 467, 412, doi: [10.1093/mnras/stx079](https://doi.org/10.1093/mnras/stx079)
- Pang, P. T. H., Tews, I., Coughlin, M. W., et al. 2021, *ApJ*, 922, 14, doi: [10.3847/1538-4357/ac19ab](https://doi.org/10.3847/1538-4357/ac19ab)
- Rappaport, S., Podsiadlowski, P., Joss, P. C., Di Stefano, R., & Han, Z. 1995, *MNRAS*, 273, 731, doi: [10.1093/mnras/273.3.731](https://doi.org/10.1093/mnras/273.3.731)
- Reddy, V., Kelley, M. S., Farnocchia, D., et al. 2019, *Icarus*, 326, 133, doi: [10.1016/j.icarus.2019.02.018](https://doi.org/10.1016/j.icarus.2019.02.018)
- Renedo, I., Althaus, L. G., Miller Bertolami, M. M., et al. 2010, *ApJ*, 717, 183, doi: [10.1088/0004-637X/717/1/183](https://doi.org/10.1088/0004-637X/717/1/183)
- Robson, T., Cornish, N. J., & Liu, C. 2019, *Classical and Quantum Gravity*, 36, 105011, doi: [10.1088/1361-6382/ab1101](https://doi.org/10.1088/1361-6382/ab1101)
- Romero, A. D., Campos, F., & Kepler, S. O. 2015, *MNRAS*, 450, 3708, doi: [10.1093/mnras/stv848](https://doi.org/10.1093/mnras/stv848)
- Schmidt, H. 1996, *A&A*, 311, 852
- Stroeer, A., & Vecchio, A. 2006, *Classical and Quantum Gravity*, 23, S809, doi: [10.1088/0264-9381/23/19/S19](https://doi.org/10.1088/0264-9381/23/19/S19)
- Tan, H., Dore, T., Dexheimer, V., Noronha-Hostler, J., & Yunes, N. 2022, *PhRvD*, 105, 023018, doi: [10.1103/PhysRevD.105.023018](https://doi.org/10.1103/PhysRevD.105.023018)
- Tang, S.-P., Jiang, J.-L., Han, M.-Z., Fan, Y.-Z., & Wei, D.-M. 2021, *Phys. Rev. D*, 104, 063032, doi: [10.1103/PhysRevD.104.063032](https://doi.org/10.1103/PhysRevD.104.063032)
- Tauris, T. M. 2018, *PhRvL*, 121, 131105, doi: [10.1103/PhysRevLett.121.131105](https://doi.org/10.1103/PhysRevLett.121.131105)
- Tauris, T. M., & Savonije, G. J. 1999, *A&A*, 350, 928, doi: [10.48550/arXiv.astro-ph/9909147](https://doi.org/10.48550/arXiv.astro-ph/9909147)
- Tauris, T. M., & Sennels, T. 2000, *A&A*, 355, 236, doi: [10.48550/arXiv.astro-ph/9909149](https://doi.org/10.48550/arXiv.astro-ph/9909149)
- Tutukov, A. V., & Yungel' Son, L. R. 1993, *Astronomy Reports*, 37, 411
- Usman, S. A., Mills, J. C., & Fairhurst, S. 2019, *ApJ*, 877, 82, doi: [10.3847/1538-4357/ab0b3e](https://doi.org/10.3847/1538-4357/ab0b3e)
- Vidaña, I., Logoteta, D., Providência, C., Polls, A., & Bombaci, I. 2011, *EPL (Europhysics Letters)*, 94, 11002, doi: [10.1209/0295-5075/94/11002](https://doi.org/10.1209/0295-5075/94/11002)
- Wolfram Research, Inc. 2024, *Mathematica*, Version 14.0, 12.3.1. <https://www.wolfram.com/mathematica>
- Yu, S., Lu, Y., & Jeffery, C. S. 2021, *MNRAS*, 503, 2776, doi: [10.1093/mnras/stab626](https://doi.org/10.1093/mnras/stab626)
- Zhou, X. R., Burgio, G. F., Lombardo, U., Schulze, H. J., & Zuo, W. 2004, *PhRvC*, 69, 018801, doi: [10.1103/PhysRevC.69.018801](https://doi.org/10.1103/PhysRevC.69.018801)
- Zurairq, Z., Mukhopadhyay, B., & Weber, F. 2023, *Astronomy Reports*, 67, S199, doi: [10.1134/S1063772923140214](https://doi.org/10.1134/S1063772923140214)

APPENDIX

A. REMARKS ON ASSUMPTIONS AND ERROR PROPAGATION

The purpose of this study is to demonstrate the the potential of utilizing GW observations to constrain NS mass in conjunction with EM observations. Therefore, we have not incorporated uncertainties in the distance to the system and in the mass of the WD. For a more rigorous analysis, these uncertainties must be explicitly included in the error propagation.

For WDs are sufficient bright in the optical wavebands, Gaia can provide accurate distance measurements. To determine the mass of a WD, as an isolated source in the field or as a component star in a binary, is less straightforward. The most widely adopted method for WD mass determination relies on the measurement of surface gravity and effective temperature by fitting spectroscopic data with atmospheric models (see e.g. Holberg et al. 1985, 1986; Bergeron et al. 1992; Bragaglia et al. 1995; Schmidt 1996; Finley et al. 1997; Barstow et al. 2001; Kepler et al. 2017). The results, combined with a theoretical mass-radius relation for finite-temperature WD structure (see e.g. Althaus et al. 2005; Renedo et al. 2010; Romero et al. 2015), enable reasonably accurate mass inferences. A complication is that whether the WD in NS-WD binaries would adhere to this evolutionary mass-radius relation, particularly in the presence of tidal effects and potential pulsar irradiation. However, when an accurate distance measurement is available, combining WD luminosity with effective temperature information allows deducing radius and, consequently, mass without detailed modelling of atmospheric physics (Koester et al. 1979; Bédard et al. 2017; Genest-Beaulieu & Bergeron 2019). Conversely, this method can also be used to derive the distance to the binary when combined with surface gravity measurement if an accurate parallax measurement is unavailable. If the WD undergoes a certain evolutionary phase, pulsation mode analysis provides accurate mass measurements (see e.g. Kawaler 1990; Bradley & Winget 1994; Córscico et al. 2019).

While a detailed analysis of the accuracy and systematics in mass and distance determination is beyond the scope of this work, we still include here a recipe for error propagation appropriate for applications in real observations. When the error bars are much smaller than unity, we can write $d = d_0(1 \pm \delta_d)$, where d_0 represents the true value of distance and δ_d represents the relative size of its error bar. The error of distance enters the GW mass function via

$$\delta_{\text{gm, re}} = \delta_{\text{gm}} + \frac{3}{5} \delta_d, \quad (\text{A1})$$

where $\delta_{\text{gm, re}}$ represents the realistic relative error bar of $g(m)$, and δ_{gm} represents the case with known distance (as used in the main text of this paper). Therefore, a 10% uncertainty of the distance translates into a 10% uncertainty of m_{ns} , approximately.

The companion mass does not enter the GW parameter estimation process, and therefore it does not affect the derived uncertainty of the GW mass function even if it is unknown. However, its uncertainty will affect the constraint on the NS's mass, as its value is used to derive m_{ns} from the intersection of two mass functions. We suppose that the companion's mass $m_c = m_{c,0}(1 \pm \delta_c)$.

When all system parameters are measured with errors much smaller than unity, Eq. 12 can be approximately solved using series expansion. Keeping all errors to the leading order, the relative error on the NS mass can be approximated as:

$$\begin{aligned} \delta_m &= C_{\text{gm}} \delta_{\text{gm, re}} + C_{\text{fm}} \delta_{\text{fm}} + C_c \delta_c, \\ &= \frac{1}{32(\cos 2\iota_0 + 3)m_{\text{ns},0} - 3m_{c,0}(-4 \cos 2\iota_0 + \cos 4\iota_0 - 61)} \\ &\quad \times \left\{ 8 \sin^2 \iota_0 (\cos 2\iota_0 + 7)(m_{c,0} + m_{\text{ns},0}) \delta_{\text{fm}} \right. \\ &\quad \left. + 5(28 \cos 2\iota_0 + \cos 4\iota_0 + 35)(m_{c,0} + m_{\text{ns},0}) \left(\delta_{\text{gm}} + \frac{3}{5} \delta_d \right) \right. \\ &\quad \left. - [2m_{c,0} (52 \cos 2\iota_0 + 3 \cos 4\iota_0 + 9) + 3(28 \cos 2\iota_0 \right. \\ &\quad \left. + \cos 4\iota_0 + 35)m_{\text{ns},0}] \delta_c \right\}, \quad (\text{A2}) \end{aligned}$$

where $C_{\text{gm}} \delta_{\text{gm, re}}$ and $C_{\text{fm}} \delta_{\text{fm}}$ are the contribution from $f(m)$ and $g(m)$, and $C_c \delta_c$ is the contribution from m_c . The coefficient $C_c \in [-0.28, 0]$ for edge-on system and ~ -1.3 for face-on system when $m_{c,0} = [0.1, 0.6] M_\odot$. Note that the orders of magnitude of all coefficients (C) are unity, indicating that the uncertainty in m_{ns} will be dominated by the measurement with the greatest uncertainty δ . To utilize this method for the precise determination of NS mass, accurate measurements of distance and the WD mass are necessary.